ELSEVIER

Chemical Physics 192 (1995) 281–294

Chemical Physics

Dynamical properties of carbonyl sulphide diluted in argon at different densities. A molecular dynamics investigation

D. Dellis, J. Samios *

University of Athens, Department of Chemistry, Laboratory of Physical Chemistry, Panepistimiopolis 157-71, Athens, Greece

Received 28 April 1994; in final form 4 November 1994

Abstract

Molecular dynamics simulation was used to study the single molecule dynamical properties of OCS diluted in argon at two temperatures and at different densities. The translational motion of OCS molecules was studied by calculating the linear velocity and the center-of-mass total force autocorrelation functions (ACFs). The rotational motion was studied in terms of the angular velocity and of the first and second order reorientational ACFs. The characteristic density dependence of both molecular motions of OCS perturbed by argon has been obtained and discussed in terms of the alternations in the shape of the ACFs. We found that the best trial function which reproduces quite satisfactory the linear and angular velocity ACFs at low and intermediate densities is one of two exponential terms with slowly decaying tails. Gordon's generalized diffusion models as well as the "Gaussian" cage model were used to analyse the rotational $C_\omega(t)$, $C_1(t)$ and $C_2(t)$ ACFs of OCS in argon from low to sufficiently high densities. We found that the most successful model in reproducing the MD rotational ACFs and especially in the sufficiently high density range, was the "Gaussian" cage model. Finally, this study has shown that the simulated first order reorientational ACFs are in successful agreement with the corresponding experimental ACFs obtained from the fundamental parallel bands of OCS in previous infrared studies of this molecular system.

1. Introduction

As a part of our studies on carbonyl sulphide (OCS) diluted in dense rare gases and liquid solvents, we investigated recently [1] the intermolecular interactions between argon and OCS. In that study, hereafter referred to as I, we pointed out that our proposed atom–atom interaction model predicts a non-linear T-shaped dimmer (OCS–Ar) structure which is in excellent agreement with experiment [2].

Moreover, using this model, the molecular dynamics (MD) technique has been applied to simulate a 2% mixture of OCS in argon at room temperature and different densities. We studied diffusion coefficients, thermodynamic properties and mainly the intermolecular structural properties of the system. It may be also mentioned that in I the effect of the density on the local intermolecular structure of OCS molecules perturbed by argon atoms has been well demonstrated and analysed.

On the other hand, it is also profitable to look at what can be learned about the dynamical properties of this system. This is the main purpose in the present MD study. Especially, in this work, we will focus our attention to the dynamics of the OCS molecules in the mixture, by investigating the behaviour of the single

* Corresponding author.

SSDI 0301-0104(94)00385-8

molecule translational and rotational motion as the system density increases.

To our knowledge, the rotational dynamics of OCS in argon under pressure have been the subject of several infrared (IR) studies in the past [3–6]. Actually, in these experimental studies, the fundamental bands ν_1, ν_2 and ν_3 of OCS molecules perturbed by argon and other small molecules at pressures up to 300 bar, have been investigated. The main purpose in the IR study [4] was the investigation of the parallel and symmetrical ν_3 band of this linear molecule in Ar, Ne and N_2, at pressures up to 1500 bar. The corresponding rotational correlation function, the spectral moments $M(2)$ and $M(4)$ and the intermolecular mean squared torques have also been determined from the band profiles. Furthermore, the density dependence of the obtained correlation functions was clearly shown and has been compared [3,6] with the usual rotational models [7–9].

On the other hand, under the frame of this MD simulation and in terms of the calculated rotational ACFs, we will try to analyse the behaviour of the translational and rotational dynamics of OCS in the mixture under these conditions. At this stage, the various ACFs concerning the dynamics of OCS will be computed and compared with the corresponding experimental and theoretical model functions.

2. Computational details

The MD simulations were performed in the microcanonical ensemble with 10 linear OCS molecules dissolved in 490 Ar atoms. The usual periodic boundary conditions have been applied. Moreover, the system has been simulated at temperatures 293 and 313 K and at 12 different densities which correspond to the pressure range between 15–925 bar.

In addition, the influence of the sufficiently high density on the dynamics of OCS in the mixture was also examined in the present work. In view of this situation, we have investigated five thermodynamic states at 293 K and at high densities which correspond to the pressure range between 3000–10000 bar.

We note that the potential model, the parameter values and the technical details of the simulation have been described in our previous treatment [1]. All simulations after achieving equilibrium were subsequently extended to 315 ps where the various time-dependent correlation functions were calculated every 8 time steps. The obtained functions are discussed in the following section. The MD runs were performed on a CONVEX C3820 two processor computer at the NSCR DEMOKRITOS, Athens, with fully vectorised code. Additional MD runs were performed on a CONVEX C3820 at the Computer Center of National University of Athens.

3. Dynamics of OCS diluted in Ar

3.1. Translational motion

The single-molecule translational motion of OCS diluted in Ar has been studied at each thermodynamic state of interest and in terms of the calculated center of mass linear velocity ACFs

$$C_v(t) = \frac{\langle \boldsymbol{v}(0) \cdot \boldsymbol{v}(t) \rangle}{\langle \boldsymbol{v}^2(0) \rangle} . \qquad (1)$$

These functions are shown for the 12 state points in Fig. 1a. Fig. 1b illustrates the $C_v(t)$ ACFs of OCS in the mixture obtained in the cases of sufficiently high densities. By inspecting the curves in Fig. 1a, it is easy to observe that the ACFs decay faster as the density increases and that in this density range they do not exhibit a negative portion. From the results in Fig. 1b we can see that above the density of 1.66 g/cm^3 ($\cong$5000 bar) these functions exhibit a negative part. Similar behaviour has been also observed in the $C_v(t)$ ACFs obtained previously in the cases of pure liquid CS_2 [10] and OCS [11]. Comparing these results to each other we may conclude that the existence of such a negative part in $C_v(t)$ ACFs is due to the density and not to the kinetic energy. Moreover, as Singer et al. pointed out in Ref. [12], in the case of high density the existence of a negative long time tail in $C_v(t)$ ACFs may be interpreted as a result due to the collective motion of the neighbouring molecules.

Although the ACFs in Fig. 1a seem to decay exponentially, however, by using a careful non-linear least-squares fit procedure based on Marquardt's algorithm [13], we find that the model function, first introduced in Ref. [12], which successfully reproduces the MD $C_v(t)$ results is that of the following form

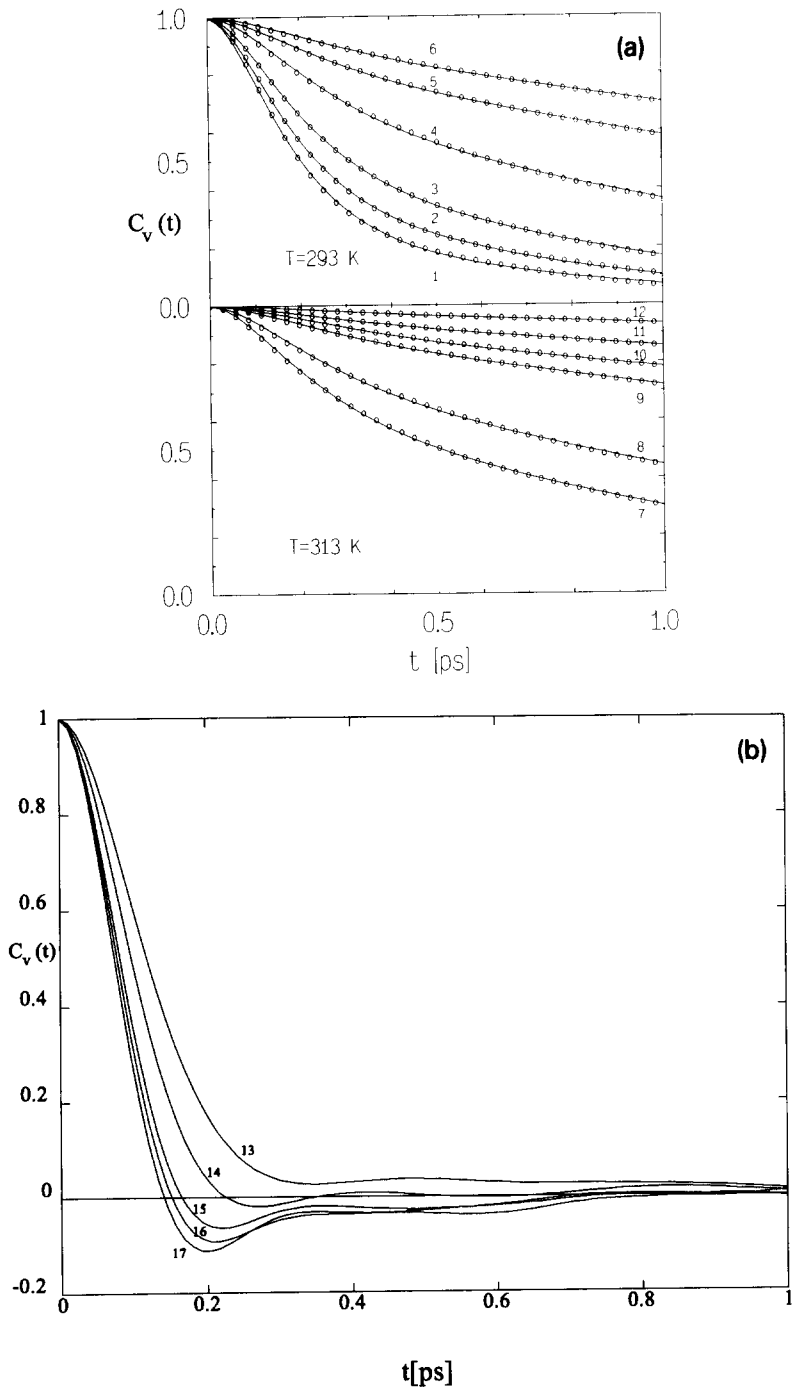

Fig. 1. (a) The linear center of mass velocity ACFs of OCS in the sample at temperature 293 and 313 K and at twelve different densities from MD runs 1 to 12 as in Table 1. The circles represent the MD results and the solid lines are obtained by the fit of the model function of Eq. (2) to these data. (b) The linear center of mass velocity ACFs of OCS in the sample at 293 K and at sufficiently high densities from MD runs 13–17 corresponding to the thermodynamic state points as in Table 1.

Table 1
Fit parameters obtained using Eq. (2) as model function for $C_v(t)$ and $C_\omega(t)$ ACFs from this MD simulation at low and intermediate densities. τ_n is the correlation time obtained by intagration of Eq. (2) using the fitted parameters. The second row corresponds to the parameters of the $C_\omega(t)$ functions

Run	T (K)	V_m (cm^3)	p (bar)	c	τ_1 (ps)	τ_2 (ps)	τ_n (ps)
1	293	41.7	925	0.247	0.094	0.395	0.331
				0.008	0.069	0.674	0.148
2	293	46.6	718	0.334	0.099	0.413	0.402
				0.049	0.078	0.353	0.183
3	293	57.4	469	0.435	0.109	0.480	0.534
				0.217	0.084	0.217	0.226
4	293	99.5	228	0.608	0.133	0.720	0.971
				0.512	0.090	0.352	0.448
5	293	172.3	133	0.764	0.142	1.074	1.695
				0.576	0.141	0.661	0.881
6	293	280	81	0.838	0.157	1.353	2.302
				0.654	0.188	1.011	1.452
7	313	82.4	313	0.583	0.122	0.613	0.808
				0.341	0.104	0.408	0.415
8	313	119.3	209	0.684	0.137	0.800	1.171
				0.614	0.099	0.374	0.536
9	313	298	83	0.844	0.155	1.456	2.489
				0.687	0.189	1.094	1.621
10	313	393	64	0.862	0.181	1.915	3.329
				0.740	0.211	1.383	2.256
11	313	590	43	0.915	0.172	2.350	4.302
				0.802	0.225	1.654	2.742
12	313	1493	17	0.961	0.178	3.701	7.084
				0.893	0.282	3.010	5.436
13	293	29.46	3000	–	–	–	–
14	293	24.06	5000	–	–	–	–
15	293	23.4	8000	–	–	–	–
16	293	22.8	9000	–	–	–	–
17	293	22.26	10000	–	–	–	–

$$C_v(t) = (1-c)(1+t/\tau_1)\ \mathrm{e}^{-t/\tau_1} + c(1+t/\tau_2)\ \mathrm{e}^{-t/\tau_2}. \quad (2)$$

This trial function has been also tested upon the calculated $C_v(t)$ ACFs in a previous MD treatment of Cl_2, Br_2, F_2 and CO_2 [12].

The simulated and fitted by Eq. (2) ACFs up to 1 ps are displayed in Fig. 1(a). The obtained values of the parameters c, τ_1 and τ_2 are summarized in Table 1. Also, the relaxation times τ_1 and τ_2 are plotted versus the reciprocal molar volume of the system in Fig. 2. As it can be seen from Table 1, by decreasing the density of the system the function $C_v(t)$ converges to a simpler one term form given by

$$C_v(t) = (1+t/\tau_1)\ \mathrm{e}^{-t/\tau_1}. \quad (3)$$

Fig. 3 shows the behaviour of these two terms in Eq. (2) as obtained by the fit procedure which was applied upon the MD $C_v(t)$ ACFs considering the cases of the lower and relatively higher densities of the system and at a temperature of 293 K.

Another point of interest here is to study the mobility of the OCS molecule parallel and normal to the molecular axis. This analysis has been applied previously in MD studies of liquid N_2, CS_2 and OCS [14,10,11]. The main conclusion from these studies was that the molecular motion parallel to the molecular axis is preferred above the motion normal to this axis.

For this purpose, the ACFs $C_v^{\parallel}(t)$ and $C_v^{\perp}(t)$ of OCS in the environment of argon atoms have been calculated at each state point of interest. Fig. 4 illustrates the behaviour of the $C_v(t)$, $C_v^{\parallel}(t)$ and $C_v^{\perp}(t)$

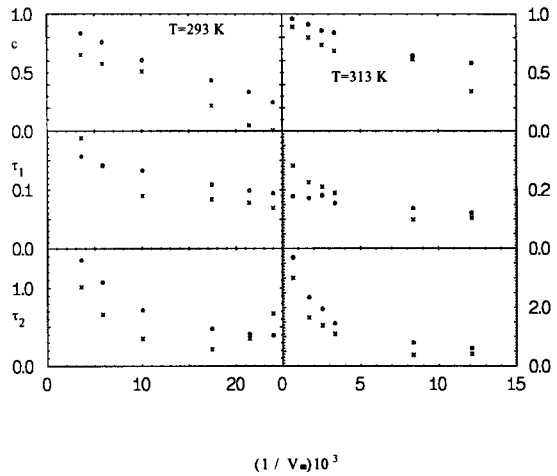

Fig. 2. The variation of the relaxation times τ_1 and τ_2 and the parameter c versus the reciprocal molar volume (V_m^{-1}) of the system obtained by the fit procedure of Eq. (2) to the MD results of the $C_v(t)$ and $C_\omega(t)$ ACFs: (○) parameters for $C_v(t)$; (×) parameters for $C_\omega(t)$ ACFs. Units as in Table 1.

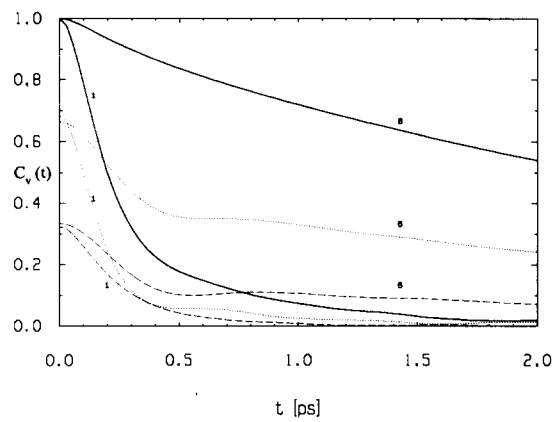

Fig. 3. The model ACF (Eq. (2)) for $C_v(t)$ obtained by the fit procedure on the MD results at 293 K and at relatively higher density (run 1) and lower density (run 6): (———) presents the total ACF, (...) presents the first term and (– – –) the second term of this function.

functions. The time dependence of these ACFs shows clear differences between the mobility parallel to and normal to the molecular axis. In this particular case we conclude that the translational motion normal to the molecular axis is preferred rather than the motion parallel to the axis. It is due to the fact that in this density range the $C_v^{\perp}(t)$ ACFs relax to zero at shorter times compared to the $C_v^{\parallel}(t)$ ACFs. This finding reveals that the motion of OCS in the environment of argon atoms at these densities, follows a different course, as opposed to its motion in the pure state at liquid densities. This finding becomes evident by direct comparison of the results in Fig. 4 with the results demonstrated in Fig. 2 of our previous paper on pure OCS [11].

In order to have some information on what can be expected relative to the force field acting on the center of mass of the linear molecule constructed from its surrounding atoms, we have calculated the center of mass force ACFs $C_F(t)$ and its components parallel and perpendicular to the molecular axis at each state point.

Fig. 5a shows some results from which it is easy to see that the center of mass ACFs $C_F(t)$ decay faster than the corresponding $C_v(t)$ ACFs. As opposed to the $C_v(t)$ ACFs, these functions exhibit a negative portion. This means that the total force acting on the OCS from the argon atoms changes in direction at a relatively short time interval more frequently than the linear velocity. However, the overall behaviour of the $C_F(t)$ may be understood if one takes into account the two components $C_F^{\parallel}(t)$ and $C_F^{\perp}(t)$ ACFs.

From the corresponding plots in Fig. 5b we see that the $C_F^{\perp}(t)$ ACF exhibits a negative part of approximately equal amplitude to the $C_F(t)$ ACF. This ACF relaxes to zero at 0.5 ps and its value at zero time is 0.8. The $C_F^{\parallel}(t)$ component has a value of 0.2 at zero time and relaxes to zero at time 0.1 ps.

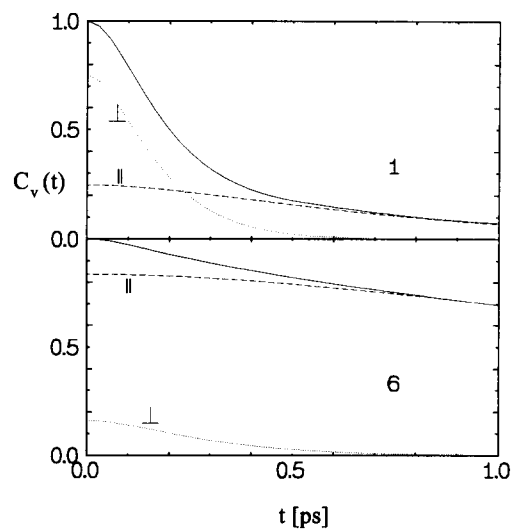

Fig. 4. The linear center of mass velocity ACFs $C_v(t)$ and the two components $C_v^{\parallel}$ and $C_v^{\perp}$ at 293 K and for MD runs 1 and 6: (———) $C_v(t)$; (– – –) $C_v^{\parallel}$; (...) $C_v^{\perp}$.

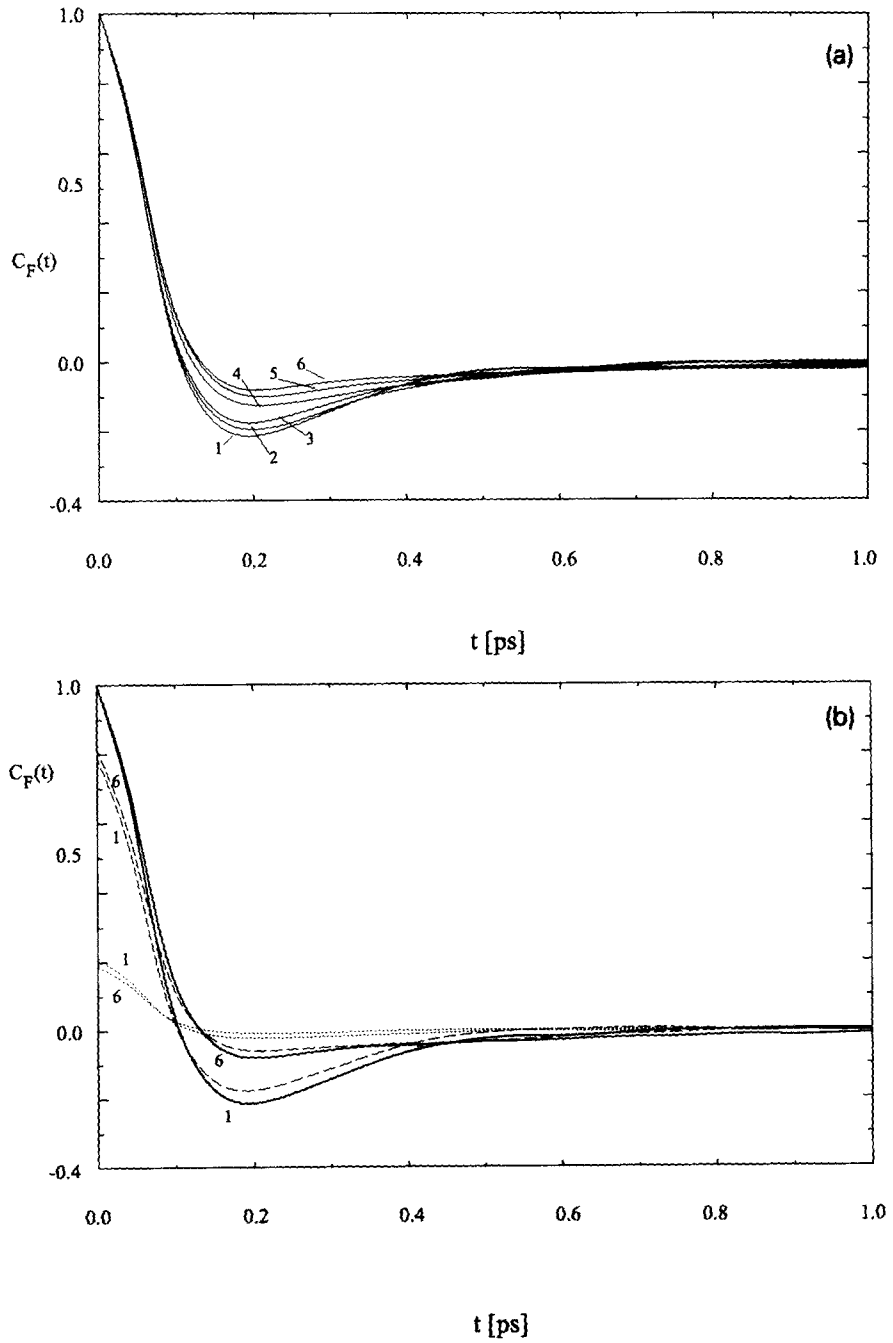

Fig. 5. The total force ACF $C_F(t)$ of OCS in argon at 293 K and different densities. (a) The curves with the number 1 to 6 correspond to the MD runs as in Table 1. (b) The total force ACFs (———) $C_F(t)$ and the two components $C_F^{\parallel}$ (...) and $C_F^{\perp}$ (– – –) at low (6) and relatively high (1) densities.

3.2. Rotational motion

The analysis of the rotational dynamics of this triatomic linear molecule in the sample is based on the most common ACFs of the angular velocity $C_\omega(t)$ and the first- and second-order Legendre reorientational ACFs $C_L(t)$ $(L=1, 2)$,

$$C_\omega(t) = \frac{\langle \boldsymbol{\omega}_i(0) \cdot \boldsymbol{\omega}_i(t) \rangle}{\langle \boldsymbol{\omega}_i^2(0) \rangle}, \tag{4}$$

$$C_1(t) = \langle \hat{\boldsymbol{u}}_i(0) \cdot \hat{\boldsymbol{u}}_i(t) \rangle, \tag{5}$$

$$C_2(t) = \tfrac{1}{2} \langle 3 | \hat{\boldsymbol{u}}_i(0) \cdot \hat{\boldsymbol{u}}_i(t) |^2 - 1 \rangle, \tag{6}$$

where $\hat{\boldsymbol{u}}_i$ represents the unit vector along the molecular axis of the OCS molecule i.

First, we will consider the angular velocity ACFs $C_\omega(t)$, which have been calculated in the same way as the linear velocity ACFs. The obtained results for the 12 state points of main interest in this work are presented in Fig. 6a, while the results of the sufficiently high densities are shown in Fig. 6b. We may easily observe that the dependence of these ACFs upon density is similar to that of the $C_v(t)$ ACFs. In other words, these ACFs decay faster as the density increases, and that in the relatively low density range (Fig. 1a) they do not exhibit a negative portion. This means that the angular velocity does not describe large alterations of its direction. However, from the results in Fig. 6b we easily observe that these functions follow a different course and they exhibit a negative part.

As in the case of the $C_v(t)$ ACFs, we fitted Eq. (2) to the simulated $C_\omega(t)$ ACFs and we found that this procedure was successful for the results corresponding to the relatively low density range (curves 1–12, Fig. 6a). The obtained parameter values are given in Table 1. From these values we may conclude that as the density increases the model function converges to the similar one-term form of Eq. (3).

At this point we must also note that our attempt to fit Eq. (2) and other trial functions to the $C_\omega(t)$ curves corresponding to sufficiently high densities was unsuccessful.

From the above results, it becomes evident that both kinds of ACFs $C_v(t)$ and $C_\omega(t)$ of the OCS molecules in argon shown in Figs. 2a and 6a (relatively low density range) may be described by the trial function of Eq. (2).

As we mentioned above, the rotational dynamics of OCS in argon have been examined by infrared spectroscopy in the past. In this case, it is well known that the total absorption coefficient $\alpha(\omega)$ at angular frequency ω is given by

$$\alpha(\omega) = \frac{4\pi^2 \omega (1 - e^{-\hbar\omega/kT})}{3\hbar k T c V_m} \int_{-\infty}^{\infty} e^{i\omega t} C_M(t)\, dt, \tag{7}$$

where c is the speed of light, V_m is the molar volume of the sample, T the temperature and $C_M(t)$ the total dipole moment correlation function of the sample

$$C_M(t) = \langle \boldsymbol{M}(0) \cdot \boldsymbol{M}(t) \rangle$$

$$= \left\langle \sum_i \boldsymbol{\mu}_i(0) \cdot \sum_i \boldsymbol{\mu}_i(t) \right\rangle. \tag{8}$$

In Eq. (8) $\boldsymbol{\mu}_i$ denotes the dipole moment of the ith molecule. The dipole moment of each molecule is the sum of the permanent $\boldsymbol{\mu}^p$ and the induced dipole moment $\boldsymbol{\mu}^i$ due to its neighbouring molecules:

$$\boldsymbol{\mu}_i = \boldsymbol{\mu}_i^p + \boldsymbol{\mu}_i^i. \tag{9}$$

It is known that the experimentally estimated value of the permanent dipole moment of the OCS molecule is 0.71 D [15]. This dipole moment $\boldsymbol{\mu}_i^p$ of OCS induces a dipole moment on each neighbouring argon atom $\boldsymbol{\mu}^{Ar,i}$ calculated by the formula

$$\boldsymbol{\mu}^{Ar,i} = \boldsymbol{\alpha}_{Ar} \nabla \frac{\boldsymbol{\mu}^p}{R^2}, \tag{10}$$

where $\boldsymbol{\alpha}_{Ar}$ denotes the polarizability of the argon atom.

This induced dipole moment of the argon atom, induces back on the OCS molecule a dipole moment $\boldsymbol{\mu}^{OCS,i}$,

$$\boldsymbol{\mu}^{OCS,i} = \boldsymbol{\alpha}_{OCS} \nabla \frac{\boldsymbol{\mu}^{Ar,i}}{R^2}, \tag{11}$$

where $\boldsymbol{\alpha}_{OCS}$ denotes the polarizability tensor of OCS molecule.

This induction mechanism has been applied in the present MD work by ignoring higher-order multipole moments of OCS molecule and first- and second field gradients. In this case we find that the induced dipole moment on OCS molecule is about 0.02 D which is negligible compared to the permanent dipole moment of OCS. Thus we neglect the possible contribution of

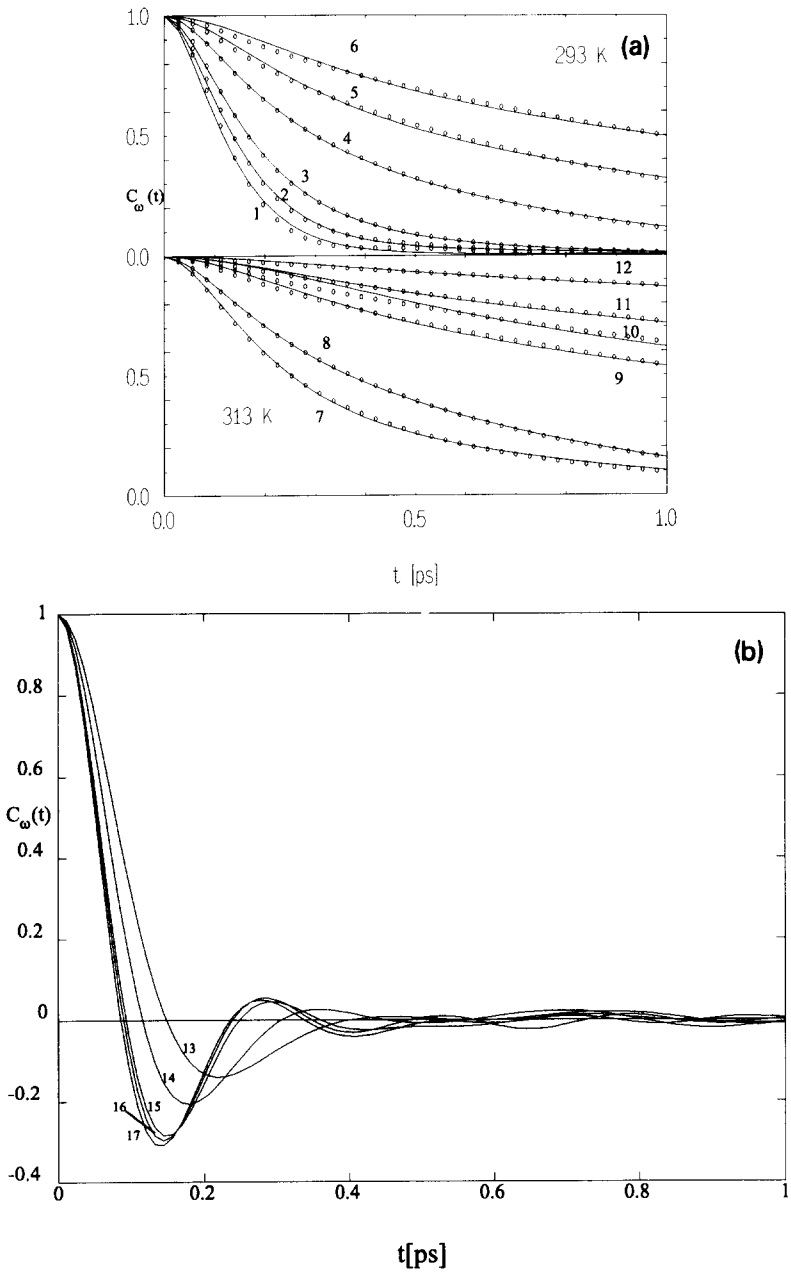

Fig. 6. (a) The angular velocity ACFs of OCS in the sample at temperature 293 and 313 K and at twelve different densities from MD runs 1 to 12 as in Table 1. Circles represent the MD results and the solid lines are obtained by the fit of the model function of Eq. (2) to these data. (b) The angular velocity ACFs of OCS in the sample at 293 K and at sufficiently high densities from MD runs 13–17 corresponding to the thermodynamic state points as in Table 1.

the induced dipole moment in the total dipole moment of the sample.

Expanding in a series the dipole moment of each molecule and neglecting higher order terms we have

$$\boldsymbol{\mu}(t) = \boldsymbol{\mu}^{\mathrm{p}} \cdot \hat{\boldsymbol{u}}(t) + \sum_l q_l(t) \cdot \left(\frac{\partial \boldsymbol{\mu}}{\partial q_l}\right)_{\mathrm{e}} + \ldots , \qquad (12)$$

where the subscript e means at zero displacement, q_l is the normal coordinate of the vibrational mode l, μ^P is the permanent dipole of the molecule and $\hat{u}$ is the unit vector along the molecular axis.

The related part for the IR spectra of the total ACFs in Eq. (5) is given by the formula

$$C_{IR}(t) = \left\langle q_l(0) \left(\frac{\partial \mu}{\partial q}\right)_e (0) \cdot q_l(t) \left(\frac{\partial \mu}{\partial q}\right)_e (t) \right\rangle . \quad (13)$$

In the case of parallel fundamental bands of OCS ν_1 and ν_3, the dipole moment derivative can be expressed as follows

$$\left(\frac{\partial \mu}{\partial q_l}\right)_e = \hat{u} \cdot \left|\frac{\partial \mu}{\partial q_l}\right|_e . \quad (14)$$

On the other hand, if we neglect the vibration–rotation interaction, the $C_{IR}(t)$ corresponding to the ν_1 and ν_3 bands can be expressed as the product of the vibrational ACF multiplied by the rotational ACF

$$C_{IR}(t) = \left\langle \left(\frac{\partial \mu}{\partial q}\right)_e (0) \cdot \left(\frac{\partial \mu}{\partial q}\right)_e (t) \right\rangle \langle q_l(0) \cdot q_l(t) \rangle . \quad (15)$$

Assuming harmonic vibrations at frequency ω_0, the time evolution of the normal coordinate q is given by $q(t) = |q| e^{i\omega_0 t}$ and by neglecting the term $e^{i\omega_0 t}$ (this means that the Fourier transform will give the spectral shape at frequencies relative to ω_0), the correlation function of interest can be written as follows

$$C_{IR}(t) = |q|^2 \left\langle \left(\frac{\partial \mu}{\partial q}\right)_e (0) \cdot \left(\frac{\partial \mu}{\partial q}\right)_e (t) \right\rangle . \quad (16)$$

Finally, Eq. (16) due to Eq. (14) takes the form

$$C_{IR}^{\nu_1,\nu_3}(t) = \left|\frac{\partial \mu}{\partial q_l}\right|^2 \langle \hat{u}(0) \cdot \hat{u}(t) \rangle . \quad (17)$$

From Eq. (17) it is expected that the parallel bands ν_1 and ν_3 must be of the same shape. This has been verified in Fig. 6 of Ref. [3] by comparing the corresponding to the ν_1 and ν_3 bands. Moreover, by normalizing the ACFs of Eq. (17) we obtain the well-known first-order Legendre reorientational ACFs for both cases by the expression

$$\nu_1, \nu_3 \text{(parallel)} \quad C_1(t) = \frac{\langle \hat{u}(0) \cdot \hat{u}(t) \rangle}{\langle \hat{u}(0)^2 \rangle} . \quad (18)$$

In the work reported here, the calculated first-order Legendre reorientational $C_1(t)$ ACFs have been compared with those obtained experimentally corresponding to the ν_1 and ν_3 IR band of the OCS molecule. The density dependence of these ACFs has been also studied.

Figs. 7a, 7b represent the obtained $C_1(t)$ ACFs which correspond to the ν_3 band at $T = 293$ and 313 K and at different densities. The inset in both figures illustrates the corresponding experimental functions obtained in the previous infrared studies [3,4] of this molecular system at the same thermodynamic conditions.

On the basis of these results, we observe a quite satisfactory agreement between these two sets (experimental and simulated) ACFs of OCS in argon. At very low densities, the corresponding ACFs (Fig. 7a, curves 4, 5, 6) display a negative part with a characteristic minimum. The depth of this minimum decreases as the density increases. It can also be observed that the rotational motion of OCS in argon becomes more restricted at densities above 300 amagat (≈ 74.7 cm^3/mol). At this and higher densities the ACFs remain positive. We also see that all ACFs relax to zero within approximately 3 ps.

In the experimental study [3], the perpendicular band ν_2 of OCS has also been investigated and the infrared bands have been obtained at pressures from 40 to 300 bar.

Following the procedure described above, the corresponding $C_1(t)$ ACF to this band takes the form

$$C_1(t) = \frac{\langle \hat{u}_\perp(0) \cdot \hat{u}_\perp(t) \rangle}{\langle \hat{u}_\perp(0)^2 \rangle} , \quad (19)$$

where $\hat{u}_\perp$ is the unit vector normal to the unit vector $\hat{u}$ defined above. Moreover, this vector at time t lies in the plane on which the triatomic molecule performs the ν_2 bending vibration.

In this particular case due to the fact that in the present MD simulation the triatomic OCS molecule has been studied as a stark without vibrations, we cannot study this band.

Clearly, much more theoretical investigation is needed in order to understand the behaviour of the ν_2 band of OCS in argon. At this stage MD simulation of the system, in which the three fundamental vibrations of the molecule have been taken into account, is under way.

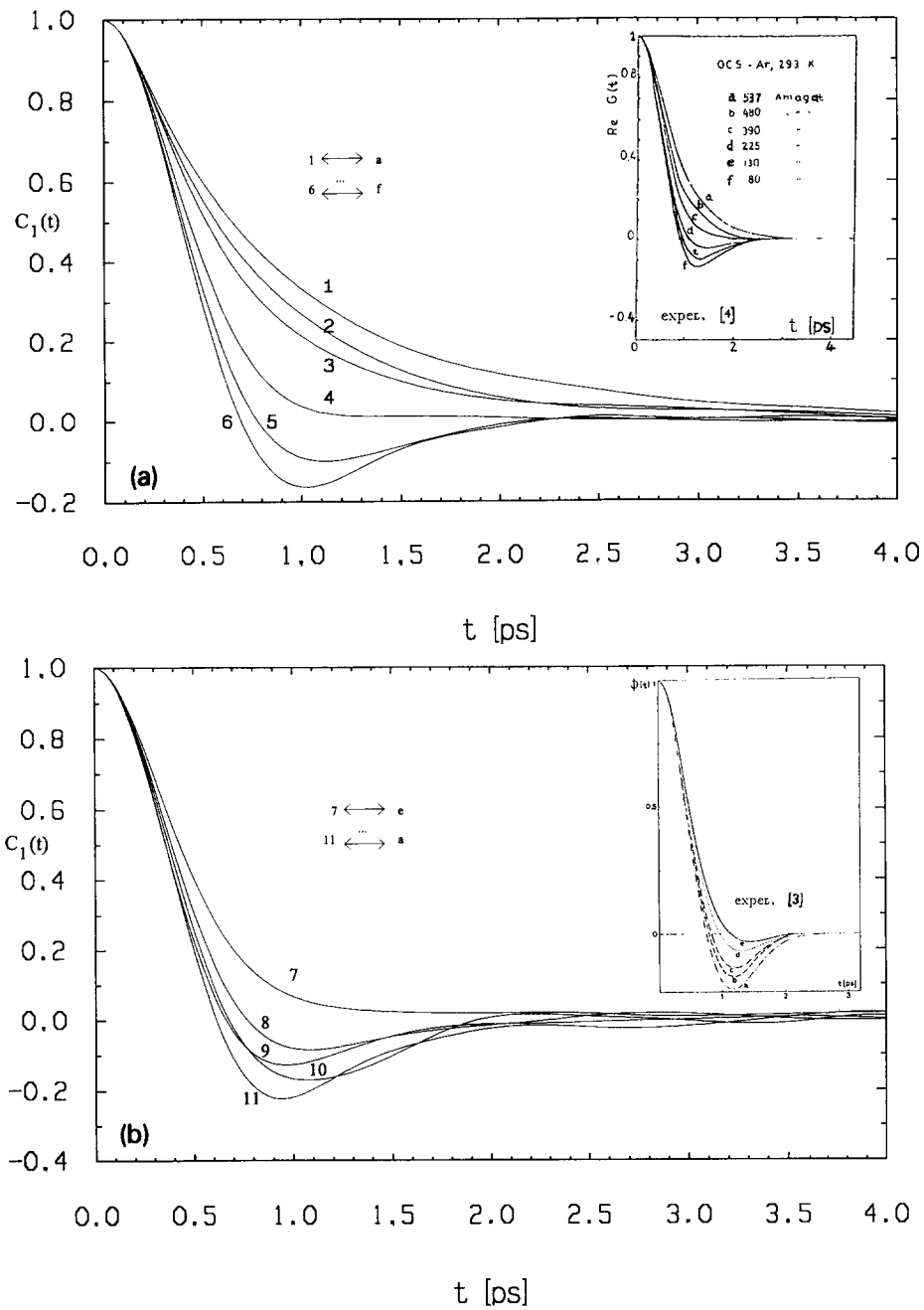

Fig. 7. The first-order Legendre reorientational ACFs at different densities corresponding to the ν_3 fundamental band of OCS in argon. The inset illustrates the corresponding experimental ACFs. The numbers on the curves indicate the corresponding MD run as in Table 1. The MD curve (1) corresponds to the experimental curve (a) etc.

Finally, in Fig. 8 we expose the reorientational second-order Legendre ACFs $C_2(t)$ of the unit vector $\hat{u}$ along the molecular symmetry axis of OCS in the sample at 293 K and at different densities. These ACFs at each MD run were computed according to Eq. (6). The obtained results show clearly a characteristic density dependence. At very low densities (curves 5, 6) the ACFs exhibit a purely free rotator behaviour. On the

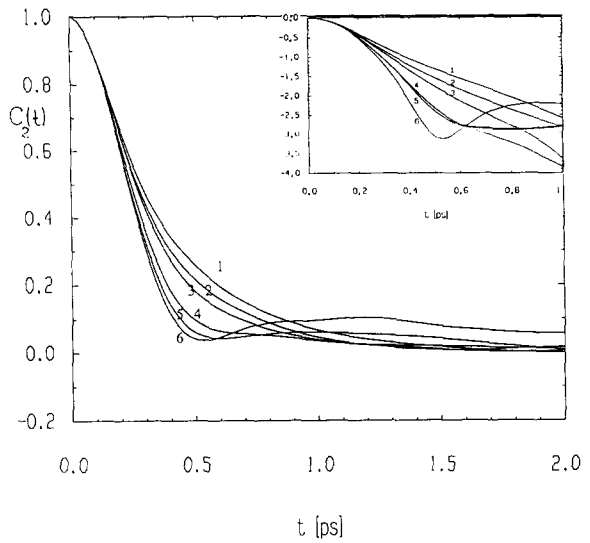

Fig. 8. The second-order Legendre reorientational ACFs of $C_2(t)$ of OCS in argon at $T=293$ K and at different densities from MD runs 1–6. The insert illustrates the semilogarithmic graphs of these functions.

other hand, as the density increases (curves 1–4) the ACFs at relatively long times show the well-known rotational diffusion as indicated by the exponential decay. This becomes evident from the inset in Fig. 8 that shows the semilogarithmic plots of $C_2(t)$ ACFs.

Unfortunately, at this and higher density range, experimental $C_2(t)$ ACFs of OCS in argon are not available in the literature. At this stage, the above MD results are very useful for future theoretical work considering the construction of models in order to describe the single molecule rotational motion as a function of the system density and, of course, of other parameters.

3.3. The M, J and Gaussian cage models

In order to analyse more precisely the rotational ACFs obtained in this MD study, the Gordon's generalized M, J [16] as well as the "Gaussian" cage model of Steele [17] have been applied.

In a previous MD study of the pure liquid OCS [11] the last model has been applied and we found that the rotational dynamics of liquid OCS may be described in terms of this model. This conclusion may be drawn from the reorientational ACFs $C_1(t)$, $C_2(t)$ as well as from the angular velocity ACFs $C_\omega(t)$.

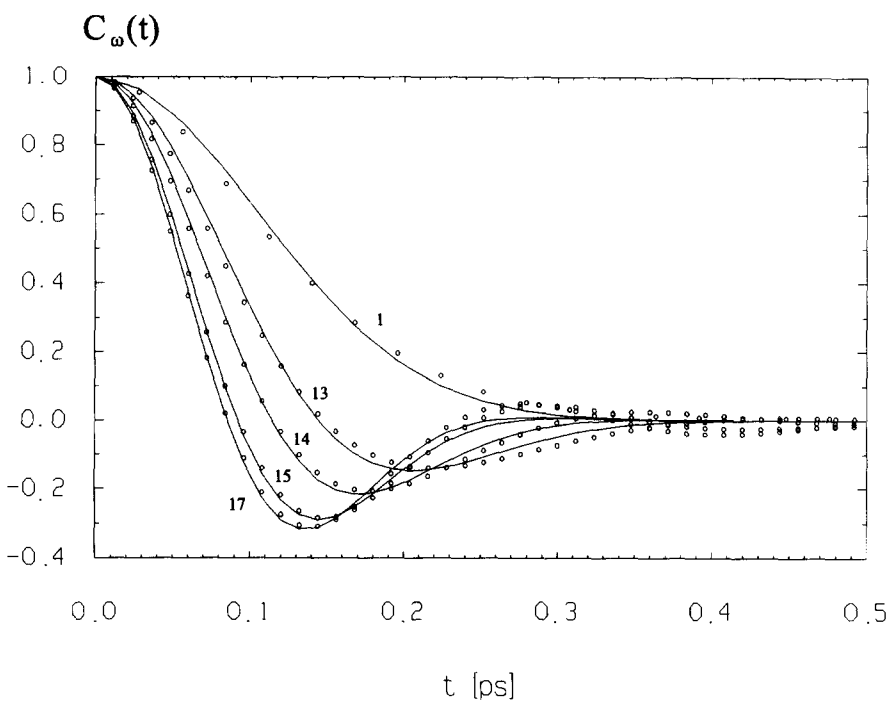

Fig. 9. The simulated angular velocity (ooo) with the Gaussian cage model (fits) ACFs, (——), at 293 K and at sufficiently high densities (MD runs 1, 13, 14, 15 and 17).

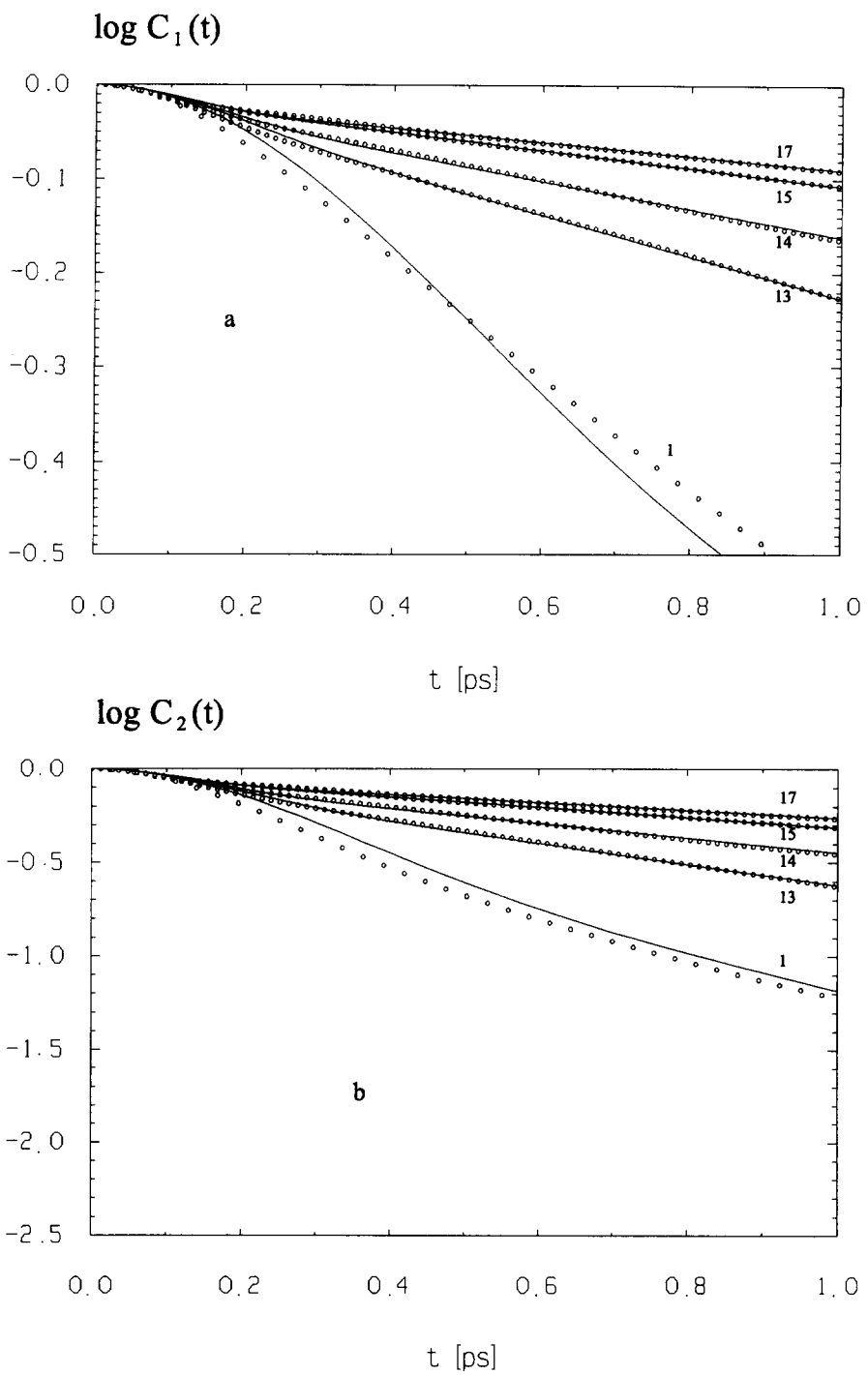

Fig. 10. The simulated a: log $C_1(t)$ and b: log $C_2(t)$ (ooo) with the Gaussian cage model (fits) (———) ACFs, at 293 K and at sufficiently high densities (MD runs 1, 13, 14, 15 and 17).

As in the previous study [11] we apply the Gaussian model for the $C_\omega(t)$ ACFs combined with cumulant theories to yield the well-known expression for the $C_1(t)$ and $C_2(t)$ reorientational ACFs.

Our investigation has shown that generally, both the M and J models provide no satisfactory account of the MD reorientational ACFs in the whole density range of interest in this study. We must note that better results have been found in the case of the M model at very low densities.

On the other hand, the cage model seems to be more interesting in the case of sufficiently high densities. The results for the $C_\omega(t)$ ACFs are shown in Fig. 9 where we have plotted the model function against the MD data. We find a satisfactory agreement between MD results and the theoretical model at high densities (corresponding to pressures above 3000 bar). However, the fit was not successful at intermediate and low densities (see curve 1 in Fig. 9).

The accuracy of the used cage model at sufficiently high densities to describe the reorientational motion of OCS in argon becomes evident from the results in Fig. 10 where the MD $C_1(t)$ and $C_2(t)$ ACFs are plotted against the cage model function.

Finally, the above results show that the rotational motion of OCS in argon is sufficiently density-dependent and it starts becoming strongly hindered from the environmental argon atoms at pressures above 3000 bar.

4. Conclusion

In the present article, the MD simulation technique has been applied to study the single molecule dynamical properties of OCS molecules diluted in argon atoms at different densities.

The molecular system has been investigated at temperatures of 293 and 313 K and at different densities corresponding to the pressure range from 40 to 930 bar. Some extra MD runs at sufficiently higher densities, corresponding to pressures up to 10000 bar, have been also applied.

Thus, the translational and rotational dynamics of OCS perturbed by this monoatomic system have been extensively analysed in terms of the relevant calculated ACFs. The density dependence of both molecular motions has been studied in detail.

Especially, we found that the reorientational first-order Legendre ACFs corresponding to the ν_1 and ν_3 (parallel) fundamental bands of OCS are in successful agreement with the experimental ACFs obtained from IR bands in previous studies.

We found that, although this molecular system was studied over a wide range of densities in the gas state, for densities above 300 amagat the behaviour of the obtained reorientational ACFs $C_1(t)$ and $C_2(t)$ of OCS in the sample show the characteristical behaviour of the corresponding function of the liquid systems.

This finding was also stated in our previous treatment [1], where such a tendency has been found in the behaviour of the investigated distribution functions $g(r)$ of the system.

Finally, the rotational dynamics of OCS in argon may be described in terms of the Steele's "Gaussian" cage model only at sufficiently high densities above 3000 bar, while investigation of the M and J Gordon's generalized diffusion models for the same function were unsuccessful in the whole density range of interest in this study.

Acknowledgement

This work was carried out within project No. 91 EΔ 111. The financial support of the Greek Ministry of Energy and Technology is gratefully acknowledged. The CPU time allocation on CONVEX C3820 of the Supercomputing Center NCSR DEMOKRITOS Athens and on CONVEX C3820 of the Computer Center of University of Athens Greece, is also gratefully acknowledged.

References

[1] J. Samios, D. Dellis and H. Stassen, Chem. Phys 178 (1993) 83.
[2] S.J. Harris, K.C. Janda, S.E. Novak and W. Klemporer, J. Chem. Phys. 63 (1975) 881.
[3] C. Dreyfus, E. Dayan and J. Vincent-Geisse, Mol. Phys. 30 (1975) 1453.
[4] D. Clermonteel, H. Vu and B. Vodar, J. Quant. Rad. Transfer 16 (1976) 695.
[5] C. Dreyfus, L. Berreby, E. Dayan and J. Vincent-Geisse, J. Chem. Phys. 68 (1978) 2630.
[6] C. Dreyfus, L. Berreby and T. Nguyen-Tan, J. Chem. Phys. 76 (1982) 755.

[7] R.G. Gordon, Adv. Magn. Reson. 3 (1968) 1.
[8] M. Fixman and K. Raider, J. Chem. Phys. 51 (1969) 2425.
[9] R.E.D. McClung, J. Chem. Phys. 73 (1980) 2435.
[10] D.J. Tildesley and P.A. Madden, Mol. Phys. 48 (1983) 129.
[11] J. Samios and H. Stassen, Chem. Phys. 170 (1993) 193.
[12] K. Singer, J.V.L. Singer and A.J. Taylor, Mol. Phys. 37 (1979) 1234;
E. Detyna, K. Singer, J.V.L. Singer and A.J. Taylor, Mol. Phys. 41 (1980) 31.
[13] P.R. Bevington, Data Reduction and Error Analysis for the Physical Sciences (McGraw-Hill, New York, 1969).
[14] J. Barojas, J. Lavesque and B. Quentree, Phys. Rev. A 2 (1973) 1092.
[15] A.A. Deakin and S.H. Walmsley, Chem. Phys. 136 (1989) 105.
[16] R.G. Gordon, J. Chem. Phys. 44 (1966) 1830.
[17] R.M. Lynden-Bell and W.A. Steele, J. Phys. Chem. 88 (1984) 6514.